Published in final edited form as:
Appl Opt. 2012 December 1; 51(34): 8262–8270.

Mode-filtered large-core fiber for optical coherence tomography

Sucbei Moon[1] and **Zhongping Chen**[2,3,*]

[1]Department of Physics, Kookmin University, Seoul 136-702, South Korea

[2]Department of Cogno Mechatronics Engineering, Pusan National University, Busan 609-735, South Korea

[3]Beckman Laser Institute, Department of Biomedical Engineering, University of California, Irvine, California 92617, USA

Abstract

We have investigated the use of multimode fiber in optical coherence tomography (OCT) with a mode filter that selectively suppresses the power of the high-order modes (HOMs). A large-core fiber (LCF) that has a moderate number of guiding modes was found to be an attractive alternative to the conventional single-mode fiber for its large mode area and the consequentially wide Rayleigh range of the output beam if the HOMs of the LCF were efficiently filtered out by a mode filter installed in the middle. For this, a simple mode filtering scheme of a fiber-coil mode filter was developed in this study. The LCF was uniformly coiled by an optimal bend radius with a fiber winder, specially devised for making a low-loss mode filter. The feasibility of the mode-filtered LCF in OCT imaging was tested with a common-path OCT system. It has been successfully demonstrated that our mode-filtered LCF can provide a useful imaging or sensing probe without an objective lens that greatly simplifies the structure of the probing optics.

1. Introduction

Single-mode fiber (SMF) has become a popular light delivery medium for the fiber-optic imaging applications where the optical signal is required to be transmitted in preserving the beam quality or the coherence property. In contrast to the multimode fiber, the transmission performance of the SMF is not vulnerable to the interference between the guiding modes because it supports a sole guiding mode. This benefit of the SMF is obtained by restricting the fiber parameters for the single-mode characteristic. The most apparent penalty is its relatively small core or the small mode field, compared to the multimode counterpart. The diameter of the fiber core hardly exceeds 10 times of the operation wavelength, which is acceptable for most of the cases but sometimes needs to be alleviated for special requirements of the application, for example, for reduced nonlinear properties.

This disadvantage of the single-mode guidance can be relaxed by adopting a mode filtering scheme, in which the power of the high-order modes (HOMs) in a multimode fiber are selectively filtered out in the middle of the link to provide a single-mode waveguide in effect. This way of extending the single-mode regime was originally studied for improving the conventional SMF in fiber-optic communications [1–6]. Recently, we applied the same method for the fiber-optic imaging application of multiphoton endomicroscopy where a large-core fiber (LCF) of low nonlinear property is demanded [7]. By using the mode-filtering scheme, an LCF of a large mode-field area was successfully developed in keeping

* Corresponding author: z2chen@uci.edu.

the single-mode transmission characteristic. The core area could be enhanced by an order of magnitude compared to that of the conventional SMF. Thismode-filtered LCF can be a versatile medium for the other imaging applications for its attractive features that the conventional SMF cannot provide.

In this research, we are extending the application area of this scheme for the optical coherence tomography (OCT) where such an LCF is attractive for simplification of the beam-probing optics. In OCT or fiber-optic reflectometry, the optic probe for imaging the sample equips a lens for focusing the light loosely at a point of the sample. As an alternative, a cleaved fiber can directly play a role of the optic probe without an objective lens for compactness and low cost [8]. This type of lensless probes seems particularly attractive for the common-path OCT imaging or sensing applications. However, the beam coming out of the fiber end diverges so rapidly for the case of the SMF that the back-reflected power from a distant point may be insufficient with a narrow effective imaging range. The measurement range along the beam axis is determined by the beam divergence characteristic of the probing optics and has been conventionally estimated by the Rayleigh range, z_R, or the confocal parameter ($2 \cdot z_R$) based on the Gaussian-beam approximation. The Rayleigh range of a beam is given by

$$z_R = \frac{\pi w_0^2}{\lambda}, \quad (1)$$

where ω_0 is the beam waist at the focus (in radius) and λ is the operation wavelength. The effective measurement range in OCT is usually said to be four times as long as the Rayleigh range of z_R. It is reasonable to take a double of z_R for the case of the lensless probe in contrast because the beam is not to be refocused with a working distance with an objective lens. Unfortunately, the standard SMF such as SMF-28 (Corning, Inc.) has a narrow Rayleigh range of ~50 μm due to the small core diameter. The effective measurement range is just ~0.1 mm and limits the applicability of this type of OCT probes. This problem can be alleviated by utilizing the LCF with a mode filter for its large core. Note that the Rayleigh range is proportional to the square of the beam waist as in Eq. (1). The effective measurement range obtained by a large core of more than twice as large as that of the standard SMF may exceed 0.4 mm in air, taking $2 \times z_R$ as the effective measurement range. This may be useful for many cases of OCT imaging. And a wider measurement range as long as ~1 mm can be achieved with further increase of the core diameter using the same principle of operation if a relatively poor transverse resolution of ~30 μm is accepted.

To take advantage of such an attractive feature of the mode-filtered LCF, we have investigated its feasibility for OCT in this research. The intrinsically wide Rayleigh range was utilized for a lensless imaging probe of OCT. For this, a commercially available LCF was used in this study (Liekki Passive-20/125, nLight Corp.), which has a core diameter of 20 μm and a cladding diameter of 125 μm with an index contrast of 0.16% (NA = 0.08). Its cutoff wavelength of the second-order mode is estimated to be located at 2.1 μm assuming the step-index profile. Three or four modes are supported by the relatively large core in the wavelength range of 1.0–1.3 μm. Because of the large core, this LCF was expected to be useful in making a lensless OCT probe with a wide imaging range if collaborating with a suitable mode filtering device.

A high level of HOM suppression is the indispensable requirement of the mode-filtered LCF used in the OCT system. The residual HOM power may produce ghost images as a consequence of different group velocities of the fiber modes if the OCT signals are partially carried by the HOMs. Thinking of the wide dynamic range of the OCT imaging, an HOM suppression of >30 dB is required to make the effect of the residual HOM power negligible.

Although a careful launching condition to the LCF alone can minimize the excitation of the HOMs up to a certain point, it probably leaves about −20 dB or a percent of the fundamental-mode power even in the favorable condition. It should be noted that the coupling loss of more than 0.1 dB (2% in lost portion) is routinely observed in typical coupling optics and the significant portion of the loss can contribute to the HOM excitation without a mode filtering means.

Several methods of mode filtering have been proposed so far and can be utilized for the purpose of this research: tapered fibers [1,2], coiled fibers [3,4], and fused couplers [5,6]. Each of them has advantages and disadvantages in terms of performance and implementation cost. Among those schemes, the fiber coil provides the easiest way with a wide degree of adjustability. It is nothing but a section of fiber coiled in a regular geometry like a solenoid. The loops of curved fiber can remove the optical power carried by the HOMs selectively from the fiber by their characteristic curvature losses as long as the fundamental mode exhibits an exclusively stronger guidance against the bending perturbation of the fiber coil. It can be realized when the number of the fiber modes is moderate, *e.g.*, less than four in linearly polarized (LP) mode designations. In the fiber-coil mode filter, the HOM suppression is easily controlled by the length of the coiled section so that the demanded level of HOM suppression is easily achieved by winding more fiber as needed. The performance factors such as the HOM suppression are predictable because the working principle relies on the macroscopic geometry of the fiber coil. The relatively narrow operation bandwidth is of minor concern for most of the OCT systems unless ultra-fine axial resolutions are required.

In this report, we have researched the use of the mode-filtered LCF for the OCT application to make a lensless OCT probe. With an LCF and a fiber-coil mode filter, a wide Rayleigh range of 0.2 mm was achieved by the cleaved end of the mode-filtered LCF by itself, which could directly act as a lensless imaging probe of OCT. The feasibility of the fiber medium in OCT imaging was verified with a simple OCT system of the common-path configuration. For the purpose, we systematically investigated the fiber-coil mode filter to meet the high HOM suppression requirement of OCT through both theoretical and experimental studies. We have found that a simple way of coiling the LCF is a suitable mode filtering scheme in terms of implementation cost, performance controllability, and evaluation easiness, and it provides a large-core SMF that is useful for the OCT imaging application.

2. Theoretical Estimation

In this section, the characteristics of the bent fiber have been theoretically investigated to find the optimal curvature radius for the fiber-coil mode filter to efficiently remove the HOM power from the LCF in keeping a low transmission loss for the fundamental mode. For the purpose, the bend loss was calculated by using the classic formula of curvature loss derived from an approximated model of the curved waveguide [9,10]. It was assumed that the fiber has a step-index profile with a cladding part of pure silica. The secondary sources of the bend loss other than the macroscopic curvature are neglected here, but will be discussed later in this report.

A. Bend Loss of a Fiber Mode

For the conventional optical fiber that consists of high-index core and low-index cladding, the condition of the single-mode guidance is expressed by

$$V=\frac{2\pi a}{\lambda}\cdot \mathrm{NA}\approx \frac{2\pi a n_1\sqrt{2\Delta}}{\lambda} \quad (2)$$

to be lower than a cutoff point of 2.405, where a is the radius of the fiber core, λ is the wavelength of operation, and NA is the numerical aperture. Here, the NA of the fiber is determined by the core-cladding index contrast $\Delta = n_1 - n_0/n_1$ where the refractive index of the core is n_1 and that of the cladding is n_0. Lowering the index contrast of Δ may allow us to get a larger single-mode core. However, the excessive bend loss turns out to be a practical drawback. The bend loss increases rapidly as the NA of an optical fiber decreases beyond a certain limit. In this context, the bend loss of a fiber is an important factor, not only because it is the key mechanism of the fiber-coil mode filter but also because the practical application has a definite margin for the bend loss of the fundamental mode. The aim of the theoretical estimation, hence, includes quantification of the bend loss that the fundamental mode experiences when the fiber is casually curved in the application system, as well as finding the optimal bend radius by which the power of the HOMs is efficiently suppressed.

We used the comprehensive formula of curvature loss that had been derived under the approximation that the field of a fiber mode is not affected by the curved geometry [10]. For a weakly guiding mode of LP_{ml}, the loss coefficient, L_{dB}, is given in the unit of dB per unit length as a result of bending the fiber with a uniform curvature radius of R as

$$L_{\mathrm{dB}}\,[\mathrm{dB}] = 4.3 \times \frac{2\sqrt{a}U^2 e^{-2W}}{e_m \sqrt{\pi} W^{5/2} R^{3/2} V^2 |H_{\mu}^{(2)}(\xi)|^2 \cdot K_{m-1}(W) \cdot K_{m+1}(W)}, \quad (3)$$

where $\mu = \beta R$ and $\zeta = n_0 k(R + a)$ with $k = 2\pi/\lambda$ are given for the guiding mode of the propagation constant β. Here, U and W are defined as $U = a \cdot \left(k^2 n_1^2 - \beta^2\right)^{1/2}$ and $W = a \cdot \left(\beta^2 - k^2 n_0^2\right)^{1/2}$, respectively. $H^{(2)}$ denotes the Hankel function of the second kind and K denotes the modified Bessel function of the second kind with the subscript to be the order. The factor of e_m is 2 for LP_{0l} modes ($m = 0$) while it equals to 1; otherwise ($m > 1$). The propagation constant β of each mode was calculated by using the scalar theory of weakly guiding fiber for this estimation [11]. It seems reasonable to take a bend loss per loop or per turn of winding ($2\pi R$ in fiber length) rather than a bend loss per unit length. Larger bends are longer in geometry when the bend or curve of fiber is made for a directional change of beam delivery. Therefore, the bend loss was evaluated by $2\pi R L_{dB}$ in dB per turn for reasonable comparison.

B. Optimal Bend Radius for Mode Filtering

The optimal bend radius for mode filtering was found by the theoretical bend loss estimation. The LCF of interest had $a = 10$ μm and $\Delta = 0.16\%$. The bend loss of the fundamental LP_{01} mode was evaluated as an insertion loss. Similarly, the bend loss of the LP_{11} mode was calculated as an HOM suppression factor. It is natural to regard the LP_{11} mode as the strongest guidance among the HOMs owing to the highest effective index. The bend loss of the LP_{11} mode, hence, can play a role of the lower bounds of the HOM suppression. Here, the fiber-coil mode filter was to be made by looping the LCF several times. The preferable number of turns in the coil was around 10 by the trade-off between the length of the LCF consumed and the adjustability of the HOM suppression factor. Hence, a turn of a fiber loop needs to give the LP_{11} mode a loss of about 3 dB to make the final HOM suppression ~30 dB.

Two different critical bend radii were defined to quantify the effects of the bend loss: the suppression-limited bend radius, R_s, and the loss-limited bend radius, R_l. The radius of R_s is defined by the largest bend radius that gives a bend loss of 3 dB per turn to the LP_{11} mode. R_l is the smallest bend radius that results in a bend loss of 0.1 dB per turn for the fundamental mode. Therefore, we could take a bend radius between those two critical radii

to make a mode filter of the optimal performances, i.e., a negligible loss to the transmitted power of the fundamental mode and a sufficiently high HOM suppression at the same time.

Figure 1 shows the calculation result of the suppression-limited bend radius and the loss-limited bend radius for optimal mode filtering with the LCF of interest. The dotted curve denotes the suppression-limited bend radius, $R_s(\lambda)$ while the solid curve denotes loss-limited bend radius, $R_l\lambda$. The shadowed area bounded by those two curves represents the optimal range for mode filtering. The radius margin was defined by $\Delta R = R_s - R_l$ to evaluate the implementation difficulty. If it were too narrow, the fiber bend would be vulnerable to the imperfect adjustments of the curvature radius and might exhibit neither a sufficient suppression for the HOMs nor a small loss for the fundamental mode. The theoretical estimation summarized by Fig. 1 suggests that our LCF had the optimum bend radius with a sufficient radius margin at $\lambda > 1.3$ μm. But it was obscured by the small radius margin at short wavelengths of $\lambda < 1.1$ μm. It is also worth stressing that this LCF can tolerate a relatively sharp bend of $R = 20$ mm with a negligible bend loss of the fundamental mode, ~0.1 dB, according to this theoretical estimation.

3. Fiber-Coil Mode Filter

A. Characterization of Bend Loss

The actual bend loss of the LCF ($2a = 20$ μm in core diameter) was measured in the experiment. We found that microbends induced by localized inhomogeneous stress may result in intermode coupling. This effect was also observed when the fiber was simply wound up around a cylindrical mandrel to make a fiber coil. Instead of this popular way of making fiber bends, a uniform curve was made in a loop by fixing the fiber minimally at a point for each turn. The uniform elasticity of the fiber kept a nearly homogeneous curvature while the microbends were reduced this way. The bend loss was measured for the fiber coil with two kinds of semiconductor optical amplifiers (SOAs) and optical power meters. The center wavelengths of the light sources were 1.05 and 1.31 μm, respectively. The transmitted power was measured as a function of the number of turns, N_t, at each wavelength. For exciting all the modes of the LCF, the light from the output SMF port of each SOA was launched into the LCF by a butt-coupling method with an intentional lateral offset of ~5 μm between the fiber cores.

Figure 2 shows the decrease of the transmitted power as the increase in the number of turns for various bend radii, measured at 1.31 (a) and 1.05 μm (b), respectively. The overall transmitted power decreased steadily as the length of the bent fiber increased at the first stage. It sometimes converged to a certain value for the cases of the moderate bend radii. This effect was clearer in Fig. 2(a) for the fiber loops of $R = 24$ mm and $R = 31$ mm. This bend-loss saturation was understood as the consequence of the HOM power depletion. Because the HOM power was rejected completely after a certain length of the bent fiber and only the power of low-order modes still remained at the core, the transmitted power becomes constant afterwards with a negligible bend loss. On the other hand, the low-order modes also experienced measurable bend losses when the bend radius was decreased further, as seen with the cases of $R = 17$ mm in Fig. 2(a). This result roughly matched the theoretical prediction that the bend radius of R between 22 and 40 mm can selectively remove the HOM power, as discussed in Fig. 1 in the previous section.

The bend-loss saturation was less clear for Fig. 2(b) of $\lambda = 1.05$ μm. The first-order saturation was observed for $R = 24$ mm, which was understood to be caused by the loss saturation of LP_{21} and LP_{02} modes. The second saturation of a smaller bend radius was observed at $R = 16$ mm, which was due to the LP_{11}-mode power depletion. But a small variation of ±1 mm in bend radius significantly changed the saturation characteristic. And a

considerable bend loss was still measured for $R = 16$ mm after $N_t \geq 4$ where the HOM power was thought to be depleted. This can be explained in part by the narrow radius margin (ΔR) at $\lambda = 1.05$ μm, which was suggested theoretically.

The experimental result described with Fig. 2 also suggests that the fundamental mode of the LCF can better tolerate the bend loss. To evaluate the minimum curvature radius that a fiber can endure, the critical bend radius, R_{3dB}, was defined as the bend radius that produces a curvature loss of 3 dB for each turn. By the loss curves of Fig. 2(a), the critical radius was estimated to be definitely below 20 mm at $\lambda = 1.31$ μm. For comparison, the bend loss of a large-core SMF was calculated by using Eq. (3). The maximum core size of SMF is defined by Eq. (2) with $V = 2.405$ for given operation wave-length and index contrast. The bend loss naturally depends on the fiber parameters and may act as a limiting factor of an SMF in practice. It was calculated that the critical bend radius becomes larger than 30 mm, which can be regarded as a bend radius of casual fiber curves, when the core diameter of an SMF exceeds 13.4 μm for $V = 2.405$ at $\lambda = 1$; 310 nm. In other words, the maximum core diameter must be no more than 13.4 μm even if accepting a considerable level of bend loss for the moderate bend radius.

On the other hand, the characteristic of the single guiding mode for the coiled LCF was confirmed by the near-field patterns imaged at the fiber end surface when the LCF was looped at the optimal bend radius. The images were acquired with a microscope objective ($NA = 0.25$) and a digital camera with the light source operating at $\lambda = 1.05$ μm. The near-field profile was acquired at $\lambda = 1.31$ μm by using a scanning microscope instead since the silicon-based image sensor does not work for the long wavelength band. The intensity profile was acquired by laterally scanning the probe fiber of a small core and high NA ($a = 0.9$ μm, NA = 0.35) on the cleaved surface of the sample LCF with a motorized translation stage while a microscope was used to measure the probing position. Figure 3 shows the microscopic images of the LCF output beam without a fiber coil (a) and with a coil in place, respectively, for $\lambda = 1.05$ μm, $R = 16$ mm and $N_t = 6$ (b). Figure 3(c) shows sity Figure the inten-profile of the LCF with a fiber coil in place for $\lambda = 1.31$ μm, $R = 26$ mm, and $N_t = 6$. A rectangle in each image represents a scale bar of 20 μm in Figs. 3(a) and 3(b). The solid curve in Fig. 3(c) is the Gaussian fit of the measured data denoted by the circular dots. The mode patterns were nearly Gaussian for the cases of the fiber-coil mode filter in place as they were the evidence of the sole existence of the LP_{01} mode in the transmitted power.

We could determine the optimal bend radius by both the theoretical estimation and the experimental evaluation as described. For a fiber-coil mode filter operating at 1.31 μm, a sufficient radius margin was given for easy implementation with the optimal bend radius of $R \approx 25$ mm. In contrast, the experimental result suggested that, for the case of $\lambda = 1.05$ μm, the efficient mode filtering may bring a considerable insertion loss to the fundamental mode. It was not yet clear whether this excessive level of the insertion loss for $R = 16$ mm was due to the fundamental limit or it was simply caused by the secondary effect of the microbends that could be reduced by adopting a better way of making bends in principle.

B. Fiber-Coil Mode Filter

A mode filter was implemented by using the optimal parameter obtained in the above, and its performance factor was evaluated for the OCT application. Concerning the way of coiling the LCF, minimization of the microbends was an important issue. Microbends were not only increasing the insertion loss of the mode filter but also inducing the intermode coupling. This kind of perturbations naturally helps the modes interchange their powers with each other. Even with a small fraction below a percent, the OCT image could suffer from the problem of ghost images that the coupled power might generate.

A fiber winder was devised for safely coiling the LCF to avoid the mode coupling effect. The transmission characteristics of the mode filter made with the fiber winder were evaluated under the offset launch condition as described earlier. Figure 4 shows the schematic diagram of the fiber winder (a) and the transmitted power as a function of the number of turns for $R = 27$ mm, measured at $\lambda = 1.31$ μm. The inset of Fig. 4(b) shows the full range of the measured data. Here, the solid line denotes the curve of an exponential decay function fitted by the measured data of the square dots in Fig. 4(b). The fiber winder equipped a circular track on the plane, which was opened partially for the sake of LCF entering and exiting the track. The LCF was placed along the inner curve of the track in a relief and kept fixed position by its own stiffness of the fiber. Three points of the thresholds were made on the circular track so that the LCF was stopped from stretching out. The LCF adhered to nowhere except for two points located just out of the track. The actual bend radius of the LCF was slightly smaller than the nominal value of $R = 27$ mm, which was, here, defined as the half of the inner diameter of the circular track.

As observed in Fig. 4(b), the transmitted power exhibited a clear saturation. The initial drop at the first two turns ($N_t \leq 2$) was dominantly caused by the loss of the LP_{21} and LP_{02}. They were rejected nearly completely for those initial turns due to the high bend loss. The curve following this rapid drop was caused by the loss of LP_{11}. The LP_{11} power decayed exponentially with a background so that the transmitted power converged to that of the LP_{01} mode. The data of $N_t \geq 2$ were fitted by an exponential decay function in a least-square manner. The fit parameters suggested the bend loss of LP_{11} was 2.04 dB per turn. After the HOM power effectively depleted for $N_t \geq 8$, the additional loss fluctuating finally reached ~0.01 dB per turn. It could be explained by the bend loss of the fundamental mode or the intermode coupling strength. After all, each turn suppressed the LP_{11} mode by 2.04 dB while the fundamental mode had an insertion loss of less than 0.01 dB per turn in average. This also clarified that our mode-filtered LCF is sufficiently bend-insensitive for $R > 27$ mm if once filtered.

With the parameters obtained in the experiment, we made a fiber-coil mode filter operating at $\lambda = 1.31$ μm. Keeping $R = 27$ mm, the number of turns was chosen as $N_t = 15$ for the mode filter to make an HOM suppression more than 30 dB. The insertion loss to LP_{01} was estimated to be small, <0.2 dB. For minimization of the microbends, the LCF was coiled slightly more softly than we did for the experiment of Fig. 4(b). The actual bend radius was a little smaller and could be said to be ~26 mm. The final mode-filtered LCF equipped the fiber-coil mode filter at a side. The length of the LCF consumed in the fiber coil was 2.5 m while the total length of the LCF was 5.5 m. On the other hand, we repeated the experiment for $\lambda = 1.05$ μm with the bend radius of $R = 16$ mm. But the obtained result was inconsistent due to the high sensitivity of the bend loss as predicted by the small bend radius margin at that wavelength band. It was found difficult to make a fiber-coil mode filter for that short-wavelength band with a good reliability.

4. Lensless OCT Probe

To confirm experimentally the wide Rayleigh range of the beam diverging from the mode-filtered LCF, the peak intensity was measured at $\lambda = 1.31$ μm with a small-core SMF as a probing fiber. The beam divergence characteristic was evaluated by the intensity profile as a function of the distance, z, from the LCF end surface. The measurement condition was the same as that of the experiment described with Fig. 3(c), except that the probe SMF scanned the beam axially along the fiber axis. Figure 5 shows the intensity decrease along the fiber axis out of the LCF: the measured data (square dots) and the best fitted Gaussian beam (dotted line) along with the relative beam diameter of the Gaussian beam (solid gray curve), for the mode-filtered LCF of $2a = 20$ μm. The beam diameter of $1/e^2$ intensity was 20.2 μm

on the fiber end surface, evaluated by the transverse intensity profile. The intensity slightly increased at $z = 0.07$ mm and the beam diameter decreased accordingly. The minimum beam diameter was found to be 18.4 μm (ω_0 9.2 μm) at that point of $z = 0.07$ mm. The Gaussian beam of ω_0 9.2 μm best matched the intensity decrease for distant points. The Rayleigh range of the Gaussian beam was estimated to be 0.20 mm while the actual half-intensity distance from the fiber end was 0.22 mm. Then, the effective measurement range was estimated to be 0.4 mm long or slightly longer in the air. On the other hand, the beam divergence characteristic of the standard SMF (SMF-28, Corning Inc.) was also evaluated for comparison. The beam was measured to exhibit $\omega_0 = 4.8$ μm and $z_R = 0.055$ mm. Compared with the SMF, the LCF had two-fold bigger a mode-field diameter and four-fold wider the resultant Rayleigh range.

To test the basic imaging performance with the mode-filtered LCF, a spectral-domain OCT or reflectometry system was constructed with the SOA operating at $\lambda = 1.3$ μm and a spectrometer. Figure 6 shows the schematic diagram of the fiber-optic reflectometer system used for this test. It could acquire A-lines without beam scanning optics just for evaluation of the basic imaging performance. The light from the SOA was launched to the LCF by a fusion splice via an SMF coupler. A fiber-coil mode filter was installed in the middle of the LCF that was used for the sample-arm fiber. There, the LCF was perpendicularly cleaved at the other end, which acted as a lensless OCT probe. The light reflected backward by the cleaved surface played a role of the reference light in a common-path configuration of OCT. The spectral interferogram of the interfered fields was acquired by the spectrometer with a resolution of ~0.05 nm. The center wavelength of the acquired spectrum was 1.3 μm with a full bandwidth of 60 nm. The spectral width of the source was 40 nm in the full width at the half maxima. The power irradiated on the sample was 0.31 mW. The reference power was estimated to be ~10 μW. It was evaluated that the fusion splice of the SMF-28 to the LCF produced an insertion loss of ~1.8 dB one way (LP_{01} only) due to the mode-field mismatch. This technical loss could be reduced if optimized coupling optics were used. The loss of the fused coupler was 1.6 dB in the path of the reflected light.

A-lines were taken by the Fourier transforms of the acquired spectra. For the analysis of the sensitivity drop, a single-point reflection was measured with a thick glass plate as a reference reflector. Besides, a thin glass plate was analyzed by the system as a demonstration of the film thickness measurement. The axial resolution of the system was evaluated to be 23.1 μm from the A-line data. Figure 7 shows the sensitivity role-off characteristic (a) and the A-line of the 0.15 mm thick glass plate (b). In both cases, the glass plates of the samples were tilted by ~4° with respect to the beam axis (denoted by θ in Fig. 6) so that the back-reflected light was efficiently coupled to the HOM to simulate a worst case of the measurement condition.

The sensitivity of the system was evaluated to be −84.9 dB from the data of no sample in place (black shadowed area in each graph). The sensitivity decreased at a rate of about 1.8 dB for every 100 μm in depth. For such a highly reflecting surface, the position could be determined at far points up to $z = 1.5$ mm. The thin glass plate was also successfully measured with a sufficient depth margin of ~1 mm. The successful demonstration of the lensless probe verified the practical effectiveness of the fiber-coil mode filter for single-mode LCF. The HOM was efficiently suppressed so that a high dynamic range of >30 dB was achieved for the OCT A-lines. It suggests that the residual HOM power was negligible and rarely re-excited by the intermode coupling that the casual bends might induce.

5. Discussion

The optimal bend radius for mode filtering, which was the primary design parameter of the fiber-coil mode filter, could be determined by evaluating the bend losses of the fundamental mode and the second-order HOM (LP_{11}) in theory or experiment as described in this report. We found that the experimental observation approximately agreed with the theoretical estimation so that the required bend radius for mode filtering could be obtained by a simple calculation based on the formula of Eq. (3). However, considerable differences were found between them in terms of the quantitative accuracy. Although the formula could predict the basic characteristic of the bend loss, the measured amounts deviated from the calculated values especially for the HOMs of the LCF. For example, the bend loss of LP_{11} for $R = 27$ mm was measured to be 2.04 dB per turn in a careful evaluation described with Fig. 4, while the theoretical prediction was >3 dB per turn as indicated by $R < R_s$ at $\lambda = 1.31$ μm in Fig. 1.

This inaccuracy of the curvature loss formula was investigated before [10,12]. The dominant portion of the error comes from the fact that the field deformation caused by the waveguide curvature was neglected in the approximation. The error is known to be more apparent for the HOMs such as LP_{11}, while it is relatively small for the fundamental mode. Exact theoretical estimation of the bend loss requires accurate information of the mode fields in the curved waveguide, which complicates the theoretical analysis. This inaccuracy could be the reason why the optimal bend radius of a low insertion loss was not experimentally found at $\lambda = 1.05$ μm in spite of the theoretical presence expected from Fig. 1. On the other hand, the theoretical estimation was found to be acceptably exact for the fundamental mode. The bend loss of LP_{01} became significant for $R < 24$ mm for $\lambda = 1.31$ μm, and $R < 16$ mm for $\lambda = 1.05$ μm in experiment. This matches well the curve of the loss-limited bend radius found in Fig. 1. Therefore, it can be recommended to use the simple formula of Eq. (3) for the first-order estimation of the optimal bend radius, which helps the subsequent experimental optimization of the design parameters.

Minimization of the microbends has been found to be of major concern in the practical implementations of the fiber-coil mode filters. In our experiment, the LCF was coiled inside a cylindrical track rather than out of a mandrel for the reduced microbends as described with Fig. 4(a). It has been observed that the microbends did not only give an additional loss to the fundamental mode but induced the mode coupling between the modes. As seen in Fig. 7(b), spurious peaks just above the noise floor were observed after the real signals. Those peaks were thought to be generated by the microbends of the fiber coil and limited the dynamic range of the system. This effect of mode coupling was thought to be the limiting factor of the mode filter with such a high HOM suppression. The whole coupling efficiency of the sample signal carried by the HOMs to the OCT system was thought to be even lower than the mode filter alone allowed by the HOM suppression (−30 dB). In consideration of the LCF-to-SMF coupling method of the fusion splice, it is reasonable to think that the spurious signal was produced by the coupled power from the HOMs to the fundamental mode in the middle of the fiber coil.

Out of the fiber coil, microbends could also be made by curving the LCF sharply or pressing it with a high pressure. Because of the different group velocities, the A-line became contaminated by clearly visible secondary peaks followed by the actual reflection peaks if the LCF was pressed at points. The position of such a spurious peak in an A-line depends on the relative modal delay that the signal experiences. The relative modal delay, Δt, of an HOM is estimated with respect to the delay of LP_{01} as

$$\Delta t = \frac{L \cdot n_{\text{eff}} \Delta}{c} \cdot \delta, \quad (4)$$

where L is the length of fiber, n_{eff} is the effective index of the LP_{01} mode, Δ is the index contrast, and c is the speed of light. Here, δ is the fractional difference of the normalized group velocity for the HOM. The corresponding spatial delay of the spurious point is calculated by $c \cdot \Delta t$ when the signal was partially transmitted by the HOM with length L. As a rule of thumb, δ can be estimated to be 0.1 ~ 0.2 for the LP_{11} mode of a step-index LCF in the range of V = 3.5–7.0 (Figure 3.12 in [11]). Taking n_{eff} = 1.45, the spatial delay was calculated to be 230 ~ 460 μm for a meter of the LCF we used in this research. In our OCT experiment, the delay of the spurious peak was experimentally measured to be 260 μm for L = 1 m when the LCF was pressed at two points with sharp edges that stimulated mode coupling.

This effect of mode coupling has been hardly observed with casual fiber bends of large bend radii above 30 mm. The spurious response that followed the real reflection peaks in Fig. 7(b) was understood as the result of continuously distributed points of mode coupling along the LCF coiled by R = 27 mm. This also suggests the macroscopically curved geometry of the LCF rarely produced spurious responses of larger than −30 dB even when cascaded multiply as in the fiber coil. But the LCF still needs to be protected with an appropriate buffer against the external inhomogeneous forces that may result in unwanted microbends for OCT. Further investigations are required on this topic for practical applications of the mode-filtered LCF in OCT imaging.

6. Conclusion

In this research, the mode-filtered LCF was made by using the fiber-coil mode filter and its effectiveness of the OCT application was tested to take advantage of the enhanced beam divergence characteristic, which may enable a lensless OCT probe with a sufficiently long effective measurement range. A long Rayleigh range of 0.2 mm or an effective measurement range of 0.4 mm was achieved with the mode-filtered LCF of $2a$ = 20 μm solely. For this, a very simple scheme of mode filtering was developed with the fiber-coil mode filter. The LCF was coiled by an optimal bend radius with a fiber winder that produced a fiber coil with reduced microbending. The optimal bend radius was found by the theoretical analysis and the experimental evaluations to fulfill the performance requirements of the mode filter for the OCT application. It is expected that optimizations of the fiber parameters for the LCF may extend the measurement range further up to ~1 mm by using the same scheme of mode filtering.

Acknowledgments

This research was supported by the WCU program (R31-20004) through the National Research Foundation of Korea funded by the Ministry of Education, Science and Technology and research program of Kookmin University.

References

1. Moon S, Kim DY. Effective single-mode transmission at wavelengths shorter than the cutoff wavelength of an optical fiber. IEEE Photon. Technol. Lett. 2005; 17:2604–2606.
2. Đonlagić D. In-line higher order mode filters based on long highly uniform fiber tapers. IEEE J. Lightwave Technol. 2006; 24:3532–3539.
3. Schnitzer P, Jager R, Jung C, Michalzik R, Wiedenmann D, Mederer F, Ebeling KJ. Biased and bias-free multi-Gb/s data links using GaAs VCSELs and 1300-nm single-mode fiber. IEEE Photon. Technol. Lett. 1998; 10:1781–1783.

4. Vez D, Hunziker SG, Kohler R, Royo P, Moser M, Bächtold W. 850 nm vertical-cavity laser pigtailed to standard singlemode fibre for radio over fibre transmission. Electron. Lett. 2004; 40:1210–1211.
5. Tian Z, Chen C, Plant DV. 850 nm VCSEL transmission over standard single-mode fiber using fiber mode filter. IEEE Photon. Technol. Lett. 2012; 24:368–370.
6. Kumar A, Ghadirli S, Thyagarajan K. Performance of a dual-mode–single-mode waveguide coupler as a modal filter. Appl. Opt. 1992; 31:5092–5095. [PubMed: 20733677]
7. Moon S, Liu G, Chen Z. Mode-filtered large-core fiber for short-pulse delivery with reduced nonlinear effects. Opt. Lett. 2011; 36:3362–3364. [PubMed: 21886211]
8. Sharma U, Kang JU. Common-path optical coherence tomography with side-viewing bare fiber probe for endoscopic optical coherence tomography. Rev. Sci. Instrum. 2007; 78:113102. [PubMed: 18052460]
9. Marcuse D. Curvature loss formula for optical fibers. J. Opt. Soc. Am. 1976; 66:216–220.
10. Marcuse D. Field deformation and loss caused by curvature of optical fibers. J. Opt. Soc. Am. 1976; 66:311–320.
11. Okamoto, K. Fundamentals of Optical Waveguides. Academic; 2000.
12. Kaufman KS, Terras R, Mathis RF. Curvature loss in multimode optical fibers. J. Opt. Soc. Am. 1981; 71:1513–1518.

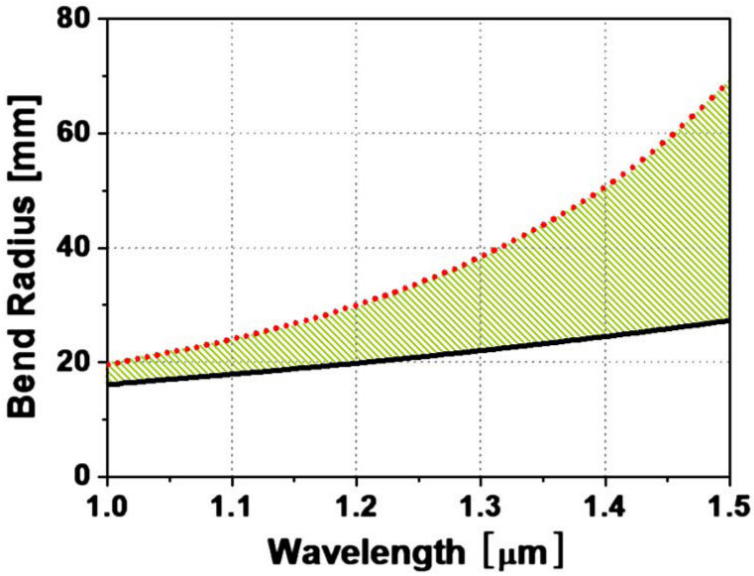

Fig. 1.

(Color online) Optimal bend radius for mode filtering bounded by the suppression-limited radius, R_s (dotted curve) and the loss-limited radius, R_l (solid curve), which were calculated with the parameters of the LCF.

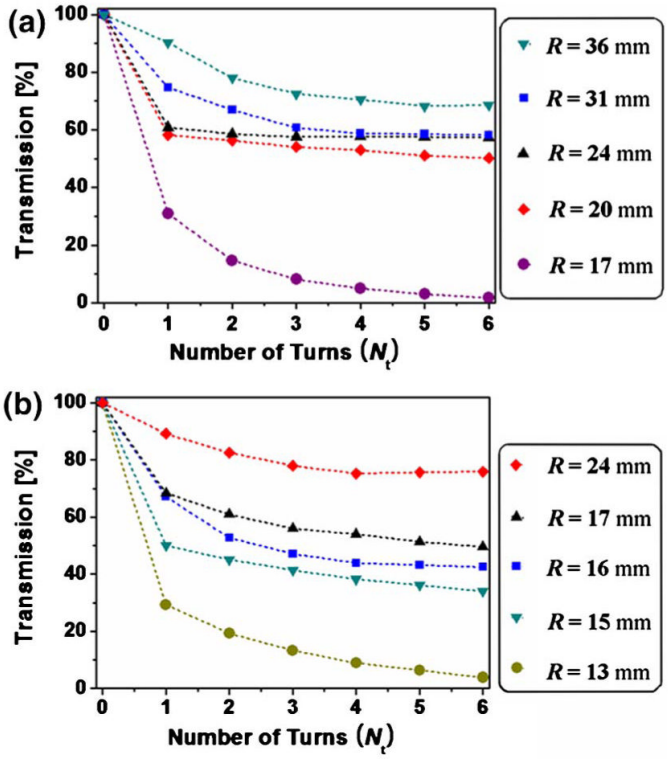

Fig. 2.
(Color online) Transmitted power of the fiber bends characterized by the number of turns (N_t) and the bend radius (R), which was measured at (a) 1.31 and (b) 1.05 μm, respectively.

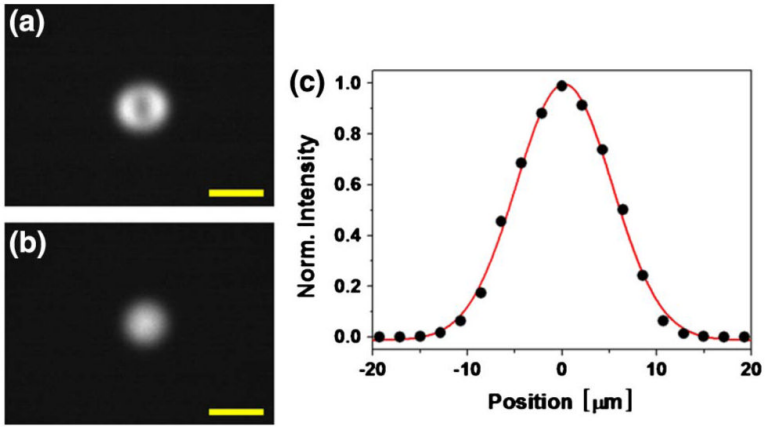

Fig. 3.

(Color online) Microscopic images of the LCF output (a) without a fiber coil and (b) with a coil in place for $\lambda = 1.05$ μm, $R = 16$ mm and $N_t = 6$, along with (c) the intensity profile with a coil in place for $\lambda = 1.31$ μm, $R = 26$ mm and $N_t = 6$.

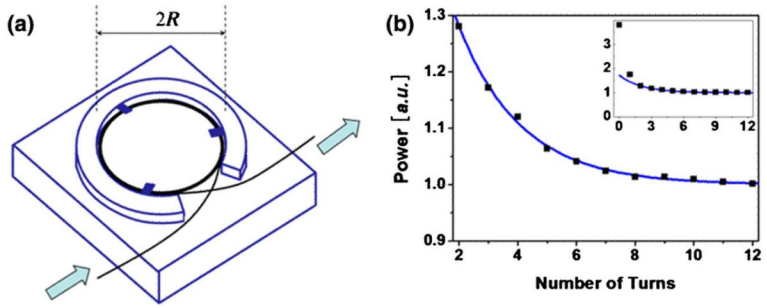

Fig. 4.

(Color online) Schematic diagram of (a) the fiber winder and (b) the transmitted power as a function of the number of turns for $R = 27$ mm, measured at $\lambda = 1.31$ μm.

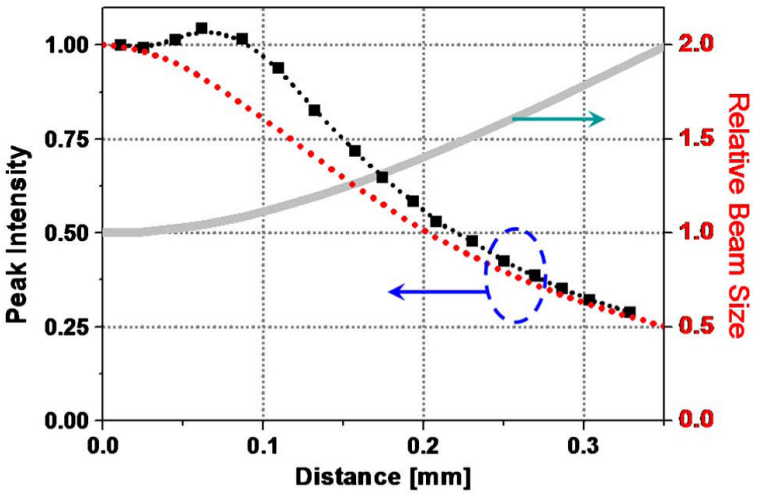

Fig. 5.

(Color online) Intensity decrease along the fiber axis out of the LCF: measured data (■) and that of the best fitted Gaussian beam (dotted curve) along with the relative beam diameter of the Gaussian beam (solid gray curve).

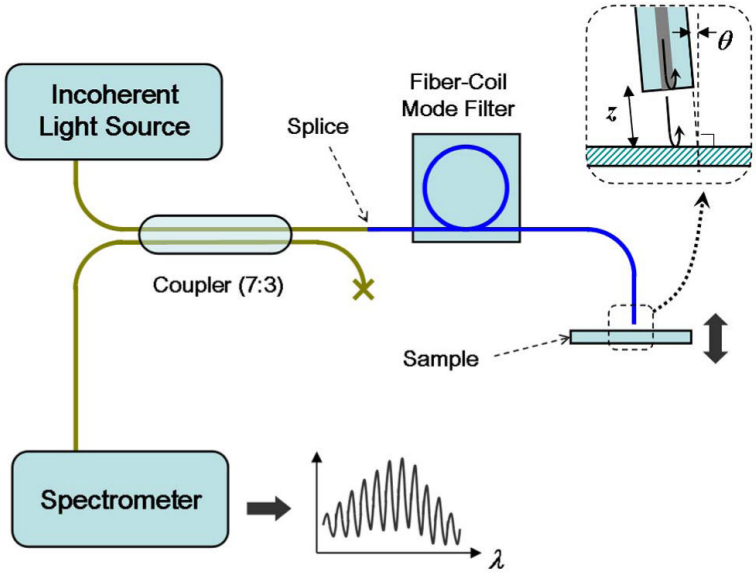

Fig. 6.
(Color online) Schematic diagram of the fiber-optic interferometric reflectometer used in the experiment.

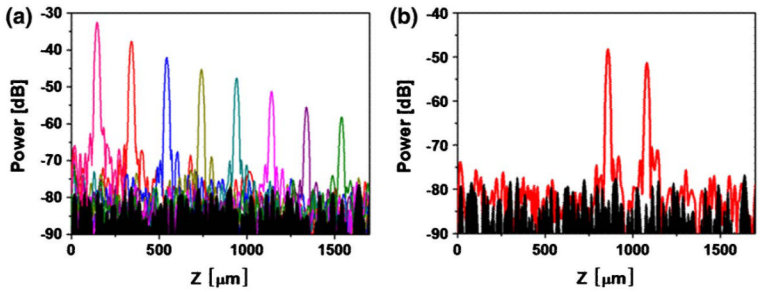

Fig. 7.
(Color online) Sensitivity role-off characteristic (a) and the reflectogram of a 0.15 mm thick glass plate (b).